International Journal of Refractory Metals and Hard Materials
Volume 95, February 2021, Article number 105441
DOI:10.1016/j.ijrmhm.2020.105441

Influence of probe geometry in micro-scale impact testing of nano-multilayered TiAlCrN/NbN coatings deposited on WC-Co

B.D. Beake[1]*, L. Bergdoll[1], L. Isern[2], J.L. Endrino[3,4], G.S. Fox-Rabinovich[5], S.C. Veldhuis[5]

1 Micro Materials Ltd, Willow House, Yale Business Village, Ellice Way, Wrexham, LL13 7YL, UK

2 School of Aerospace, Transport and Manufacturing, Cranfield University, Bedford, MK43 0AL, UK

3 Basque Center for Materials, Applications & Nanostructures, UPV/EHU Science Park, Barrio Sarriena s/n, 48940 Leioa, Spain

4 IKERBASQUE, Basque Foundation for Science, Maria Diaz de Haro 3, 48013 Bilbao, Spain

5 Department of Mechanical Engineering, McMaster University, 1280 Main Street West, Hamilton, Ontario L8S 4L7, Canada

* Corresponding author. Tel: +44 1978 261615, Fax: +44 1978 356966. Email: ben@micromaterials.co.uk

Keywords:- micro-impact, fatigue, wear, hard coatings, cemented carbide.

Abstract

Hard nano-multilayered TiAlCrN/NbN coatings on cemented carbide have shown promise in dry high speed machining applications involving repetitive contact, such as end milling of hardened H13 steel. In this study the fracture resistance of TiAlCrN/NbN coatings under repetitive dynamic high strain rate loading has been evaluated by the micro-scale impact test

method. Although the fatigue mechanisms can vary with the ratio of coating thickness t to the indenter radius R, macro-scale tests of thin coatings using probe radii in the mm range are necessarily at low t/R. Micro-impact tests at higher t/R have been performed with a range of diamond indenter geometries (R = 8, 20, 100 µm) to investigate the role of varying t/R (0.03-0.375) on the deformation behaviour. With the largest radius probe there was no clear failure for the coatings or substrate under the test conditions. With the 8 and 20 µm radius probes the behaviour of the coatings was strongly load-dependent and they were more susceptible to impact-induced damage than the carbide substrate. As the load increased there was a change from coating to substrate dominated deformation behaviour as the stress field extended further into the substrate. At lower load the dominant fracture behaviour was coating fracture through ring cracking, radial cracking and chipping. At higher load chipping became less prevalent and break-up of the carbide substrate more extensive.

1. Introduction

Multilayer coatings have shown enhanced performance in tribological tests and machining applications [1-15]. Interlinked factors responsible for the improvement include (i) higher mechanical properties, especially H^3/E^2 (ii) through-thickness graded properties (iii) crack resistance - multiple interfaces providing the ability to deflect cracks laterally rather than through-thickness (iv) rotation of columnar grains distorting bilayer period (v) interfaces providing enhanced thermal stability (vi) adaptive mechanisms from tribo-film formation. Despite generally improved performance, their behaviour at higher load can be compromised as materials with high H^3/E^2 necessarily have less available options for reducing stress by plastic deformation. Impact resistance is important for many of these applications, but it is commonly assessed through macro-scale cyclic impact/fatigue tests [16-27], with relatively

blunt (typically R = 1-3 mm) probes or nano-scale repetitive impact testing with very sharp (typically R ~50 nm) cube corner diamond indenters [14-15, 28-31]. Strong correlation between fracture resistance in the nano-impact test and cutting tool life has been reported [14-15, 28-31]. In an impact test, the severity of the test and positions of peak impact-induced stresses relative to the coating-substrate interface can be controlled by varying the applied load, accelerating distance and the probe geometry. The position of peak stresses relative to the coating-substrate interface is completely different in the nano- and macro-scale tests. FIB cut cross-sections through nano-impact test craters on multilayer TiAlSiN coatings on hardened steel revealed extensive chipping but there was no delamination [13].

To fill the gap between the nano- and macro-scale, a micro-impact test has been developed which uses impact loads in the micro- range (~0.5-5 N) together with spheroconical diamond probes with end radii of ~20 μm [32-36]. The maximum energy that can be supplied per micro-impact is x100 greater than in nano-impact. By increasing the energy delivered per impact, blunter indenter geometries can be used to produce damage within short experimental timescales. Switching from sharp to blunter spherical indenters provides an intrinsic suitability for examining gradual damage processes [16]. However, as probe radii increase, the results become progressively less sensitive to coating properties [37] and become more strongly influenced by the substrate hardness and toughness, as has also been reported in erosion testing under severe conditions [38].

In comparison to macro-scale tests, there are potential benefits of assessing coating fatigue resistance with nano or micro-impact tests. Short-duration experiments with automatic scheduling of test matrices on single samples enable rapid screening to evaluate the performance of novel coating compositions. The tests have the flexibility to alter loading level and severity of impact loading so that peak stresses can be positioned in the coating or at interface rather than in the substrate when results are less sensitive to coating properties.

The tests are depth sensing, enabling accurate recording of cycles to failure and providing information on the fatigue failure mechanism. In contrast, macro-impact tests are limited by not being depth-sensing, so the precise time at which the coating failed is not clearly defined and it is only possible to say that the coating has survived or failed after the test is ended. The failure criterion can be arbitrary with average measures such as failure area at a given number of cycles being used or the coating wear depth at the end of the test. However, as the substrate deformation may not be fully elastic to deconvolute the coating wear from substrate plasticity requires FIB cross-sectioning. Due to the large size of the test probe, the response is averaged out over a larger area of the coating surface, making it insensitive to situations where the fatigue behaviour varies across a sample. Differences between the new micro-impact test, nano-impact and conventional macro-scale impact testing are summarised in Table 1.

The micro-impact test has been used to study the impact resistance of monolayer AlTiN and TiAlCrN coatings on cemented carbide [32], mono- and multilayer TiAlSiN coatings on cemented carbide [33], graded DLC coatings on hardened steel [34] and uncoated cemented carbides [35-36]. A strong sensitivity of the damage tolerance on the applied load was reported in all these studies, which used diamond indenters of end radius ~20 μm as the impact probe. With these indenters it was possible to produce severe damage within 5-10 min tests on all the samples tested.

In this current study, TiAlCrN/NbN coatings have been used as a model system to develop our understanding of the micro-impact technique, to study the evolution of damage in repetitive small-scale mechanical contact with probes of different sharpness. TiAlCrN/NbN is a promising coating for high speed machining of hardened steels, with longer tool life than other nano-laminated coatings [1-3]. In this application the coating system displays adaptive behaviour forming beneficial tribo-oxides. These complex ($AlO_x/CrO_x/NbO_x$) tribo-films

work in synergy by protecting the surface (like alumina tribo-films), lubricating the cutting zone (like chromia tribo-films) and dissipating energy (like NbO_x films) [1]. To understand whether enhanced crack resistance from the multi-layer structure could also be important, results in the micro-impact are compared to tests on monolayer coatings (TiAlCrN) with similar mechanical properties. The results were also compared with tests on the uncoated cemented carbide substrate under the same conditions to understand the influence of substrate fatigue on the response of coated system.

2. Experimental

2.1 Samples

$Ti_{0.25}Al_{0.65}Cr_{0.10}N$/NbN nanomultilayer coatings were supplied by Kobe Steel Ltd. They were deposited using a hybrid coating system with combined plasma-enhanced cathodic arc source and unbalanced magnetron sputtering unit, using a powder metallurgical $Ti_{25}Al_{65}Cr_{10}$ alloy as target for the arc cathode and Nb as the sputtering target. Further details are given in refs [1-3]. Three compositions were tested, which varied in the power supplied to the sputter source (0.5, 1 and 2 kW) which influenced the total amount of Nb in the coating (approximately 2, 4 and 8 at.% respectively). The coatings are referred to as 0.5W, 1W, 2W. Final thickness was ~3 μm. The TiAlCrN layers were ~15 nm thick and the NbN thickness varied with the power applied to the sputtering source, so that the 2 kW were thickest. XRD data shows the nano-multilayered coatings consisted of alternating layers of fcc TiAlCrN and NbN composed of hexagonal δ' NbN with some cubic δ NbN [1]. The coatings were deposited onto cemented carbide SPG422 cutting tool inserts. The central (~4 mm diameter) circular region of the flat face of the coated insert remained uncoated and was used to assess the substrate behaviour in

the micro-impact testing. XRD showed dominant WC peaks, smaller Co/Co oxide peaks with no other refractory metals present. EDX showed 5 wt.% Co.

2.2 Nanoindentation and micro-impact testing

Nanoindentation and micro-impact tests were performed with a NanoTest Vantage system (Micro Materials Ltd, Wrexham, UK) calibrated for load, displacement, frame compliance and indenter shape in accordance with ISO14577-4. Nanoindentation was performed with a Berkovich diamond indenter whose area function was calibrated by indentation into fused silica. On each sample there were at least 10 repeat indentations to 25 mN maximum load, loading at 2.5 mN/s with a 2 s hold at peak load before unloading at 2.5 mN/s. Thermal drift correction was from a 60 s hold at 90 % unloading. Hardness and reduced elastic modulus were determined from power-law fitting to the unloading curves. The elastic modulus and Poisson ratio of the diamond indenter were 1141 GPa and 0.07 respectively. The reduced indentation moduli were converted to Elastic moduli assuming a Poisson ratio of 0.25.

Micro-impact tests were performed with a NanoTest Vantage with a loading head modified for impact testing as described in references [32-36]. The loading head was actuated with a large electromagnet capable of pulling the probe >50 µm away from the sample surface. Three spheroconical indenters with different end radii were used as impact probes in this study: (i) a spheroconical diamond indenter with 90° cone angle and calibrated end radius of 20 µm (ii) a spheroconical diamond indenter with 90° cone angle and calibrated end radius of 8 µm (iii) a diamond test probe with approximately 100 µm end radius. The end radii were calibrated by nanoindentation into a fused silica reference sample. The load is applied when the indenter is separated from the test surface by the accelerating distance and the load is maintained throughout the impact process. After the probe comes to rest it is retracted and the surface re-impacted at the same position, at 4 s intervals. The applied load and accelerating

distance control the impact energy delivered to the sample. The accelerating distance (AD) was set at 40 µm unless otherwise specified. The test duration was 300 s with 1 impact every 4 s, resulting in 75 impacts in total. Tests with the 20 µm probe were performed at 0.25 N intervals from 0.75 to 2.25 N. Tests with the 8 µm probe were performed at 0.2, 0.3, 0.5 and 1 N. Additionally, on 0.5W there were tests at 0.1 and 0.2 N with 20 µm AD. 300-1200 s tests with the ~100 µm probe were performed at 1-2.5 N. For each set of conditions there were three repeat tests in all cases.

In the micro-impact test there is a quasi-static indentation before the first actual impact. The on-load indentation depth (h_0) associated with this is recorded and is used to confirm that the depth zero is measured correctly and the test did not impact in an anomalous region of the surface. Subsequently the probe depth is recorded "on-load" for every impact. Convenient parameters for graphical illustration of the repeatability of the technique and its sensitivity to the applied load are:- (i) on-load initial static indentation depth, h_0; (ii) the on-load impact depth after the first impact, h_1; (iii) the on-load impact depth at the end of the test, h_f. h_1 is larger than h_0 as the dynamic impact force is larger than the static impact load.

Electron microscopy images were obtained using TESCAN Vega3 SEM and a TESCAN Lyra3 FIB/SEM with the secondary electron detector, 20 kV, and at a working distance of 10 mm.

3. Results

The nanoindentation data summarised in Table 2 show that the mechanical properties of the three nano-multilayer TiAlCrN/NbN coatings were very similar, all being harder but less stiff than the WC-Co substrate. The H/E ratio of the coatings was virtually the same although H^3/E^2 values were marginally higher for 0.5W and 1W than 2W.

SEM images of impact craters produced with the 20 µm probe are shown in Figure 1. All three TiAlCrN/NbN coatings showed the presence of some unreacted metal microdroplets from the TiAlCr target, which are formed during the cathodic arc deposition. There were some surface scratches from the substrate polishing prior to deposition and some porosity due to holes due to detachment of microdroplets. At 0.75 N, single or concentric ring cracks were observed with ~3 µm long radial cracks, which were more numerous on 2W. At higher load, more extensive fracture behaviour (chipping, break-up of the carbide skeleton) was observed. At 1.25 N on 1W there were more radial cracks and at 1.5 N chipping around the impact crater. At 2.25 N there was extensive break-up of the carbide skeleton at the edge of the impact crater and re-embedding of the WC in the crater.

Illustrative graphs of impact depth vs. number of impacts at each impact load are shown for 1W in figure 2 (a) and for the uncoated carbide substrate in 2(b). Corresponding depth increases (i.e. setting depth after first impact to 0) are shown in figs. 2 (c,d). 0.5W and 2W show similar results to 1W when tested with the 20 µm probe so, for simplicity, only the results on 1W are discussed in detail. During the first few impacts the depth increases rapidly, gradually slowing to approach a plateau where the depth is almost unchanged with each successive impact. The depth stabilised more rapidly at low load and the near-constant depth continued to the end of the tests (e.g. 0.75, 1.25 N in figs. 2(c,d)). More rapid increases in impact depth are observed after a period of continued impact in some tests on the coatings from ~1-1.5 N but these were absent in almost all the tests on the uncoated WC-Co. For the test in Fig. 2(a,c) the transitions are after ~50 impacts at 1.5 N, ~20 impacts at 1.75 N and ~7 impacts at 2.25 N. In several tests the transition to a more rapid removal rate was preceded by a small decrease in impact depth (as can be seen in the tests at 1.75 and 2.25 N in fig. 2 (c)). The rapid damage rate was observed in all tests on the coatings at 1.75 N and above but was

not observed for the uncoated WC-Co. Table 3(a) summarises the mean increase in impact depth during the final 10 impacts of the tests.

The load dependence of the impact parameters h_0, h_1 and h_f are shown in Figure 3 (a-b) for 1W and uncoated WC-Co respectively. For 1W, 1.5 N marks the transition to fracture (see Figs. 1(e) and 2(a)), where the increase in depth after the first impact increases by over a factor of 2 and there is greater variability in the final depth (Fig. 3(a)). For the uncoated carbide, 1.5 N also marks a transition to greater h_f-h_1 but the increase is much smaller (Fig 3(b)). The impact parameters h_0, h_1 and h_f for 1W and uncoated WC-Co are shown in Figure 3 (c)-(e). The pre-contact depth h_0 was higher throughout the load range on 1W. Until 1.25 N, h_1 was also higher on 1W, but at higher load there was no difference to h_1 on the substrate. A transition to a stronger damage mode at ≥1.5 N on the coating was not found in the tests on the uncoated WC-Co so h_f remained relatively low throughout the load range. Additional tests on the uncoated WC-Co were performed for 600 s at 2 N to investigate whether a transition occurred after more impact cycles [38]. There was a gradual increase in damage rate reaching (17 ± 11) nm/impact for the last 10 impacts.

With the sharpest probe the failure occurred at lower load. SEM images of impact craters from tests at 0.1-1 N with the sharper 8 µm end radius probe are shown in Figure 4. The SEM images show chipping at 0.1 N, 20 µm AD (Fig. 4(a)), chipping and carbide-skeleton break-up at 0.2 N (Fig. 4 (b,c)) and predominantly carbide break-up at 1 N (Fig. 4(d)). The variation in impact depth with number of impacts on 0.5W with the 8 µm probe at 0.1-1 N is shown in Figure 5. At 0.1-0.3 N after an initial increase in depth there is a plateau where the increase in depth is small until there is a transition to faster damage rate from ~32 impacts at 0.1 and 0.2 N and from ~17 impacts at 0.3 N. The mean increase in impact depth during the final 10 impacts of the tests is summarised in Table 3(b). The variation in final impact depth with the 8 µm probe at 0.2-1 N is shown in Figure 6. Additional tests at 0.1 and 0.2 N were performed

on 0.5W, lowering the AD from 40 µm to 20 µm. Under these conditions the damage with 0.2 mN and 20 µm AD was similar to that produced by 0.1 mN and 40 µm AD. At 0.1 mN and 20 µm AD the transition to a significantly faster damage rate did not occur although there were occasional small depth decreases, which are consistent with the small lateral fractures observed in figure 4(a). With the ~100 µm probe optical microscopy revealed some slight surface damage but without a clear impact crater. It was not possible to produce dramatic failure within the range of impact loads used even when tests were run over 20 min, although these showed a very gradual increase in depth with continued impacting.

4. Discussion

The mechanical properties of the hard multilayer coatings were broadly consistent with previous reports on similar coatings [1]. In monolayer hard coatings, alloying TiAlN with significant NbN has been reported to reduce elastic modulus whilst keeping hardness approximately constant [39], Although similar behaviour might be expected for TiAlCrN, the small fraction of Nb of these TiAlCrN/NbN coatings did not result in clear differences between them. Although there were some slight differences between them, in the following discussion of their impact behaviour as a function of test probe geometry and applied load it is possible to consider them together.

Probe geometry

The ratio between the coating thickness t and probe radius R has a significant influence on the deformation behaviour in spherical indentation of coated systems [40]. The probe radius clearly has at least as strong influence on behaviour in the cyclic tests as illustrated by figure 7 which compares 1 N tests with the three probes on 0.5W. Macro-scale impact tests are usually performed at low values of t/R (e.g. ~0.001) whilst nano-impact tests typically use a

cube corner which is pyramidal at the depths in the test but the effective t/R ratio is of the order of ~10. In micro-scale impact tests, t/R is intermediate between nano-impact and macro-scale impact tests. In the current study, this parameter has been varied between 0.03 and 0.375.

With the ~100 µm probe (t/R = 0.03) the impacts were almost elastic. Since it occurs in the same part of the contact region in repeat tests the surface damage is most likely to be related to imperfections on the probe which act as stress concentrators and sites for preferential damage. Within the range of available load and accelerating distance it was not possible to produce significant damage across the contact region in these short tests. With the larger probe the peak stresses move into the substrate. Substrate plasticity is reduced and the mechanical properties of the film itself do not influence the elasto-plastic deformation of the substrate so that deformation is the same for the coatings and uncoated substrate. In macro-impact tests with even lower t/R a high-cycle coating (or substrate) fatigue process may occur, with highest tensile stresses very close to the edge of the contact and blistering inside the impact zone [24-25]. However, this was not observed during the low number of cycles in the short micro-impact tests.

With the 20 µm probe (t/R = 0.15) the behaviour of the three coatings was strongly load-dependent and they were all more susceptible to impact-induced damage than the carbide substrate. To quantify the differences in behaviour of the coatings to that of the uncoated substrate, the impact parameters h_0, h_1 and h_f for 1W and uncoated WC-Co are shown in Figure 3 (c)-(e). The pre-contact depth h_0 was higher throughout the load range on 1W due to its lower elastic modulus. At 0.75-1.25 N, h_1 is also higher on 1W, presumably for the same reason, but at higher load there was no difference to h_1 on the substrate as the influence of the coating contribution to the impact stress field lessens.

Fracture occurred within 75 impacts throughout the load range with the sharpest probe (t/R = 0.375) at AD = 40 µm. The applied load and accelerating distance control the impact energy delivered to the sample. To a first approximation the impact energy is given by the product of the impulse force and accelerating distance, which was 0.2-1 x 10^{-4} J per impact in these tests. High resolution analysis of single impacts by Qin et al [41] has provided an indication of the fraction of the impact energy which is transferred to the sample and the fraction lost through transmission into the pendulum, vibration and air damping. They determined the fraction of transferred energy in nano-impact was ~0.7, and that this was almost independent of load and accelerating distance, particularly at higher load where air damping was minimal. Assuming the same fraction holds in micro-impact, the available impact energy for sample deformation was of the order of 1.4-7 x 10^{-5} J per impact. Although the absolute magnitude of the impact energy is quite low, it is acting over a very small volume so the energy densities are high when using the smaller probes (estimated to be of the order of 10 GJ/m^3) resulting in rapid fracture. In the additional tests at AD = 20 µm on 0.5W, the most fracture resistant coating in the tests with the sharp probe, only at 0.1 N and 20 µm AD was it possible to avoid the transition to a significantly faster damage rate, although lateral fracture was not completely suppressed.

Load dependent impact fracture behaviour

In impact tests with the 8 and 20 µm probes SEM imaging confirms a clear load-dependent change from coating to substrate dominated deformation behaviour. At lower load the dominant fracture behaviour is coating fracture. Damage at lower load proceeds by a three stage process: (1) ring cracking, (2) radial cracking (3) chipping. The presence of droplets on the surface from the arc deposition process may act as stress raisers promoting fracture onset. There is a transition to more substrate-dominated modes as load increases and the stress field extends further into the substrate, with chipping becoming less prevalent at higher load and

carbide break-up more extensive. At the highest load there is a further more extreme deformation involving further WC fragmentation and re-embedding. With the smallest probe this behaviour occurs from the lowest load. Figure 5 shows that as the test progressed and the contact pressure decreased the rate of increase in impact depth gradually slowed down and the rate of increase during the last 10 impacts (Table 2(b)) actually decreased as the load increased for all the coatings but not for the uncoated WC-Co.

The marked sensitivity in the micro-impact tests on the load and probe radius is consistent with what has been observed in nano-impact with sharp cube corner probes where results are even more dominated by the coating properties. Chipping in nano-impact can be extensive, but significant delamination is not commonly observed on strongly adherent coatings [13]. In a contact fatigue study of TiN coated WC-10 wt.% Co at 200-900 N with a 1.25 mm radius WC-Ni indenter, Tarrés and co-workers noted [16] that the damage mechanism proceeded by (i) nucleation of surface circular cracks after plastic deformation of the substrate (ii) growth of these through the coating thickness (iii) substrate cracking without any intermediate interface delamination. In the intermediate regime in the micro-impact test there is more interfacial failure, although this is accompanied by significant coating and substrate damage.

Although 0.5W showed the best performance at lowest load with the sharpest probe (Figure 6), and with the 20 µm probe (see low wear rate at 0.75 and 1 N in Table 3(a)) in general the behaviour of all three coatings was very similar at higher load. This may reflect the greater influence of the WC-Co substrate as the load increases. The slightly less consistent impact behaviour of the 2W coating may be related to its slightly lower H^3/E^2. Higher H^3/E^2 can improve resistance to fracture initiation due to enhanced load support reducing bending stresses. Better performance for the 0.5W at low load could be due to a combination of high H^3/E^2 and larger number of interfaces (due to thinner NbN layers). There were only small differences between the impact behaviour of nano-multilayered TiAlCrN/NbN to

monolayered PVD TiAlCrN and AlTiN coatings on hard cemented carbide substrate tested [32] with a 17 μm radius probe. These coatings had very similar H^3/E^2 values (0.099-0.108 GPa), with a slightly thicker coating with highest H^3/E^2 performing best. The similar behaviour suggests there is little microstructural advantage in the nano-multilayers under these conditions and impact resistance is controlled by the mechanical properties of the coating-substrate system.

5. Conclusions

Micro-impact tests with a range of diamond indenter sharpness (R = 8, 20, 100 μm) and applied load have shown how the dimensionless parameter t/R influences the deformation behaviour. With the 100 μm probe there was no clear failure for the coatings or substrate under the test conditions. With the 8 and 20 μm radius diamond probes the behaviour of the TiAlCrN/NbN nano-multilayer coatings was strongly load-dependent and they were more susceptible to impact-induced damage than the carbide substrate. As the load increased there was a change from coating to substrate dominated deformation behaviour. At lower load the dominant fracture behaviour was coating fracture. Damage at lower load proceeded by a three-stage process: (1) ring cracking, (2) radial cracking (3) chipping. There was a transition to more substrate-dominated modes as load increased and the stress field extended further into the substrate, with chipping becoming less prevalent at higher load and carbide break-up more extensive.

6. Acknowledgements

Funding to develop the novel micro-impact test technique through the Innovate UK Project No: 132369 – "Nano-to Micro-Impact Testing: An in-situ test for UK SEAC sector" is gratefully acknowledged. C. Kimpton and X.W. Liu (both Cranfield University) are both acknowledged for their technical assistance with the SEM imaging and M. Rueda-Ruiz (IMDEA, Spain) is thanked for useful discussions on impact energy quantification.

References

1. G.S. Fox-Rabinovich, K. Yamamoto, A.I. Kovalev, S.C. Veldhuis, L. Ning, L.S. Shuster, A. Elfizy, Wear behaviour of adaptive nano-multilayered TiAlCrN/NbN coatings under dry high performance machining conditions, Surf. Coat. Technol. 202 (2008) 2015-2022.
2. L. Ning, S.C. Veldhuis, K. Yamamoto, Investigation of wear behaviour and chip formation for cutting tools with nano-multilayered TiAlCrN/NbN PVD coating, Int. J. Mach. Tools. Manuf. 48 (2008) 656-665.
3. A. Kovalev, D. Wainstein, G. Fox-Rabinovich, S.C. Veldhuis, K. Yamamoto, Features of self-organization in nanostructuring PVD coatings on a base of polyvalent metal nitrides under severe tribological conditions, Surf. Interface Anal. 40 (2008) 881-884.
4. Y.X. Ou, J. Lin, H.L. Che, W.D. Sproul, J.J. Moore, M.K. Lei, Mechanical and tribological properties of CrN/TiN multilayer coatings deposited by pulsed dc magnetron sputtering, Surf. Coat. Technol. 276 (2015) 152-159.
5. C. Mendibide, P. Steyer, J. Fontaine, P. Goudeau, Improvement of the tribological behaviour of PVD nanostratified TiN/CrN coatings – an explanation, Surf. Coat. Technol. 201 (2006) 4119-4124.

6. C. Mendibide, J. Fontaine, P. Steyer, C. Esnoul, Dry sliding wear model of nanometer scale multi-layered TiN/CrN PVD hard coatings, Tribol. Lett. 17 (2004) 779-789.
7. J.J. Roa, E. Jiménez-Pique, R. Martínez, G. Ramírez, J.J. Tarragó, R. Rodríquez, L. Llanes, Contact damage and fracture micromechanisms of multi-layered TiN/CrN coatings at micro- and nano-length scales, Thin Solid Films 571 (2014) 308-315.
8. X. Zha, F. Jiang, X. Xu, Investigating the high frequency fatigue failure mechanisms of mono and multilayer PVD coatings by the cyclic impact tests, Surf. Coat. Technol. 344 (2018) 689-701.
9. Y.-Y. Chang, H.-M. Lai, Wear behaviour and cutting performance of CrAlSiN and TiAlSiN hard coatings on cemented carbide cutting tools for Ti alloys, Surf. Coat. Technol. 259 (2014) 152-158.
10. Y.-Y. Chang, C.-J. Wu, Mechanical properties and impact resistance of multi-layered TiAlN/ZrN coatings, Surf. Coat. Technol. 231 (2013) 62-66.
11. Q. Zhang, Y. Xu, T. Zhang, Z. Wu, Q. Wang, Tribological properties, oxidation resistance and turning performance of AlTiN/AlCrSiN multilayer coatings by arc ion plating, Surf. Coat. Technol. 356 (2018) 1-10.
12. A.A. Vereschaka, S.N. Grigoriev, Study of cracking mechanisms in multi-layered composite nano-structured coatings, Wear 378-379 (2017) 43-57.
13. J. Chen, R. Ji, R.H.U. Khan, X. Li, B.D. Beake and H. Dong, Effects of mechanical properties and layer structure on the cyclic loading of TiN-based coatings Surf. Coat. Technol. 206 (2011) 522-529.
14. G.S. Fox-Rabinovich, B.D. Beake, K. Yamamoto, M.H. Aguirre, S.C. Veldhuis, G. Dosbaeva, A. Elfizy, A. Biksa, and L.S. Shuster, A.Y. Rashkovskiy, Structure, properties and wear performance of nano-multilayered TiAlCrSiYN/TiAlCrN

coatings during machining of Ni-based aerospace superalloys, Surf. Coat. Technol. 204 (2010) 3698-3706.

15. G.S. Fox-Rabinovich, K. Yamamoto, B.D. Beake, A.I. Kovalev, M.H. Aguirre, S.C. Veldhuis, G.K. Dosbaeva, D.L. Wainstein, A. Biksa and A.Y. Rashkovskiy, Emergent behavior of nano-multilayered coatings during dry high speed machining of hardened tool steels, Surf. Coat. Technol. 204 (2010) 3425-3435.
16. E. Tarrés, G. Ramírez, Y. Gaillard, E. Jiménez-Piqué and L. Llanes, Contact fatigue behaviour of PVD-coated hardmetals, Int. J. Refract. Met. Hard Mater. 27 (2009) 323-341.
17. M. Antonov, I. Hussainova, F. Sergejev, P. Kulu, A. Gregor, Assessment of gradient and nanogradient PVD coatings under erosive, abrasive and impact wear conditions, Wear 267 (2009) 898-906.
18. K.-D. Bouzakis, A. Siganos, T. Leyendecker and G. Erkens, Thin hard coatings fracture propagation during the impact test, Thin Solid Films 460 (2004) 181-189.
19. S. Lamri, C. Langlade, G. Kermouche, Damage phenomena of thin hard coatings submitted to repeated impacts: influence of the substrate and film properties, Mater. Sci. Eng. A 560 (2013) 296-305.
20. J.L. Mo, M.H. Zhu, A. Leyland, A. Matthews, Impact wear and abrasion resistance of CrN, AlCrN and AlTiN PVD coatings, Surf. Coat. Technol. 215 (2013) 170-177.
21. C.P.O. Treutler, Industrial use of plasma-deposited coatings for components of automotive fuel injection systems, Surf. Coat. Technol. 200 (2005) 1969-1975.
22. M.D. Bao, X.D. Zhu, J.W. He, Evaluation of the toughness of hard coatings, Surf. Eng. 22 (2006) 11-14.
23. X. Zhu, H. Dou, Z. Ban, Y. Liu, J. He, Repeated impact test for characterisation of hard coatings, Surf. Coat. Technol. 201 (2007) 5493-5497.

24. F. Ledrappier, C. Langlade, A.-B. Vannes, Y. Gachon, Damage phenomena observed on PVD coatings subjected to repeated impact tests, Plasma Process. Polym. 4 (2007) 5835-5839.

25. F. Ledrappier, C. Langlade, Y. Gachon, A.-B. Vannes, Blistering and spalling of thin hard coatings submitted to repeated impacts, Surf. Coat. Technol. 202 (2008) 1789-1796.

26. L.S. Qiu, X.D. Zhu, S. Lu, G.Y. He and K.W. Xu, Quantitative evaluation of bonding strength for hard coatings by interfacial fatigue strength under cyclic indentation, Surf. Coat. Technol. 315 (2017) 303-313.

27. L. Qiu, X. Zhu, G. He and K. Xu, The repeated spherical indentation test: an efficient way to evaluate the adhesion of hard coatings, Surf. Eng. 32 (2016) 578-584.

28. K.-D. Bouzakis, F.Flocke, G. Skordaris, E. Bouzakis, S. Geradis, G. Katirtzoglou and S. Makrimallakis, Influence of dry micro-blasting grain quality on wear behaviour of TiAlN coated tools, Wear 271 (2011) 783-791.

29. G.S. Fox-Rabinovich, B.D. Beake, S.C. Veldhuis, J.L. Endrino, R. Parkinson, L.S. Shuster, M.S. Migranov, Impact of mechanical properties measured at room and elevated temperatures on wear resistance of cutting tools with TiAlN and AlCrN coatings, Surf. Coat. Technol. 200 (2006) 5738-5742.

30. B.D. Beake, J.F. Smith, A. Gray, G.S. Fox-Rabinovich, S.C. Veldhuis, J.L. Endrino, Investigating the correlation between nano-impact fracture resistance and hardness/modulus ratio from nanoindentation at 25-500ºC and the fracture resistance and lifetime of cutting tools with $Ti_{1-x}Al_xN$ (x = 0.5 and 0.67) PVD coatings in milling operations, Surf. Coat. Technol. 201 (2007) 4585-4593.

31. G.S. Fox-Rabinovich, S.C. Veldhuis, K. Yamamoto, MH. Aguirre, A. Kovalev, D.L. Wainstein, B.D. Beake, J.L. Endrino, D.L. Wainstein, A.Y. Rashkovskiy, Design and

performance of AlTiN and TiAlCrN PVD coatings for machining of hard to cut materials, Surf. Coat. Technol. 204 (2009) 489-496.

32. B.D. Beake, L. Isern, J.L. Endrino, G.S. Fox-Rabinovich, Micro-impact testing of AlTiN and TiAlCrN coatings, Wear 418-419 (2019) 102-110.
33. B.D. Beake, A. Bird, L. Isern, J.L. Endrino, F. Jiang, Elevated temperature micro-impact testing of TiAlSiN coatings produced by physical vapour deposition, Thin Solid Films 688 (2019) 137358 (9pp).
34. B.D. Beake, T.W. Liskiewicz, A. Bird, X. Shi, Micro-scale impact testing - A new approach to studying fatigue resistance in hard carbon coatings, Tribol. Int. 149 (2020) 105732 (10pp).
35. N. Cinca, B.D. Beake, A.J. Harris, E. Tarrés, Micro-scale impact testing on cemented carbide, Int. J. Refract. Met. Hard Mater. 84 (2019) 105045 (9pp).
36. B.D. Beake, L. Isern, A.J. Harris, J.L. Endrino, Probe geometry and surface roughness effects in microscale impact testing of WC-Co, Mater. Manuf. Proc. 35 (2020) 836-844.
37. G. Ramírez, A. Mestra, B. Casas, I. Valls, R. Martínez, R. Bueno, A. Góez, A. Mateo, L. Llanes, Influence of substrate microstructure on the contact fatigue strength of coated cold-work tool steels, Surf. Coat. Technol. 206 (2012) 3069-3081.
38. M. Bromark, P. Hedenqvist, S. Hogmark, The influence of substrate material on the erosion resistance of TiN coated steels, Wear 186-187 (1995) 189-194.
39. M. Mikula, D. Plašienka, D.G. Sangiovanni, M. Sahul, T. Roch, M. Trucklý, M. Gregor, L. Čaplovič, A. Plecenik, P. Kúš, Toughness enhancement in highly NbN-alloyed Ti-Al-N hard coatings, Acta Mater. 121 (2016) 59-67.

40. J. Michler, E. Blank, Analysis of coating fracture and substrate plasticity induced by spherical indentors: diamond and diamond-like carbon layers on steel substrates, Thin Solid Films 381 (2001) 119-134.
41. L. Qin, H. Li, X. Shi, B.D. Beake, L. Xiao, J.F. Smith, Z. Sun, J. Chen, Investigation on dynamic hardness and high strain rate indentation size effects in aluminium (110) using nano-impact, Mechanics of Materials 133 (2019) 55-62.

Tables

Table 1 Comparison between different types of impact test

	Nano-impact	Micro-impact	Macro-impact
Depth-sensing	Y	Y	N
Accurate time-to-failure	Y	Y	N
Test duration	5-10 min	5-10 min	Extended duration
Test probe material	Diamond [14-15, 28-31]	Diamond	WC-Co, hardened steel, Si_3N_4 [16-25]
Test probe radius	~100 nm	5-100 µm	1-3 mm [16-25]
Coating thickness ÷ test probe radius	~10	~0.1	~0.001
Sensitivity to coating mechanical properties	High	High	may be low [36]
Sensitivity to adhesion	Medium	High	may be low [26,27]
Automatic scheduling of multiple tests	Y	Y	N
Applied load (N)	0.001-0.2	0.1-5	>>100 [16-27]

Table 2 Nanoindentation data

	H/GPa	*E*/GPa	*H*/*E*	H^3/E^2 (GPa)
0.5W	28.1 ± 5.6	470.0 ± 78.1	0.060	0.104
1W	29.6 ± 3.8	507.0 ± 77.4	0.060	0.104
2W	27.9 ± 4.2	473.2 ± 71.8	0.059	0.099
WC-Co	23.9 ± 4.2	621.5 ± 76.6	0.036	0.038

Table 3 Rate of increase in impact depth over last 10 impacts[#]

(a) *R* = 20 µm probe

	0.75 N	1 N	1.25 N	1.5 N	1.75 N	2 N	2.25 N
0.5W	0.3 ± 0.2	0.0 ± 0.1	6 ± 10	11 ± 6	35 ± 25	26 ± 26	98 ± 13
1W	0.0 ± 0.5	1.9 ± 2.2	5 ± 9	23 ± 23	18 ± 6	38 ± 42	57 ± 9
2W	0.6 ± 0.7	5 ± 8	14 ± 17	1.6 ± 0.4	49 ± 30	84 ± 14	72 ± 47
WC-Co	-0.1 ± 0.7	0.4 ± 0.4	0.5 ± 0.2	1 ± 0.5	4 ± 1	5 ± 3	2 ± 1

[#] in nm per impact

(b) *R* = 8 µm probe

	0.2 N	0.3 N	0.5 N	1.0 N
0.5W	53 ± 21	51 ± 22	34 ± 12	23 ± 4
1W	58 ± 18	85 ± 30	35 ± 1	28 ± 6
2W	48 ± 22	52 ± 19	35 ± 13	34 ± 17
WC-Co	1 ± 0	5 ± 1	76 ± 33	39 ± 17

Figure Captions

1. SEM images of impact craters with the 20 µm probe. (a) 0.75 N on 0.5W, x7000 magnification; (b) 0.75 N on 2W, x4000 magnification; (c-f) 1W x4000 magnification – (c) 0.75 N; (d) 1.25 N; (e) 1.5 N (f) 2.25 N.

2. Variation in impact depth with number of impacts with the 20 µm probe at 0.75, 1.25, 1.5, 1.75 and 2.25 N on (a) 1W (b) uncoated WC-Co; corresponding depth increases are shown in (c-d).

3. Load dependence of impact parameters h_0, h_1 and h_f in tests with the 20 µm probe on (a) 1W (b) uncoated WC-Co. Comparison between 1W and uncoated WC-Co for impact parameters (c) h_0 (d) h_1 (e) h_f.

4. SEM images of impact craters on 0.5W with the 8 µm probe. (a) 0.1 N, AD = 20 µm, x10000 magnification (b) 1.0 N, x4000 magnification. (c) 0.2 N, x5000 magnification with (d) corresponding back-scattered image.

5. Variation in impact depth with number of impacts on 0.5W with the 8 µm probe at 0.1-1 N.

6. Variation in final impact depth with the 8 µm probe at 0.2-1 N.

7. Influence of probe radius on behaviour. 1 N on 0.5W.

Figures

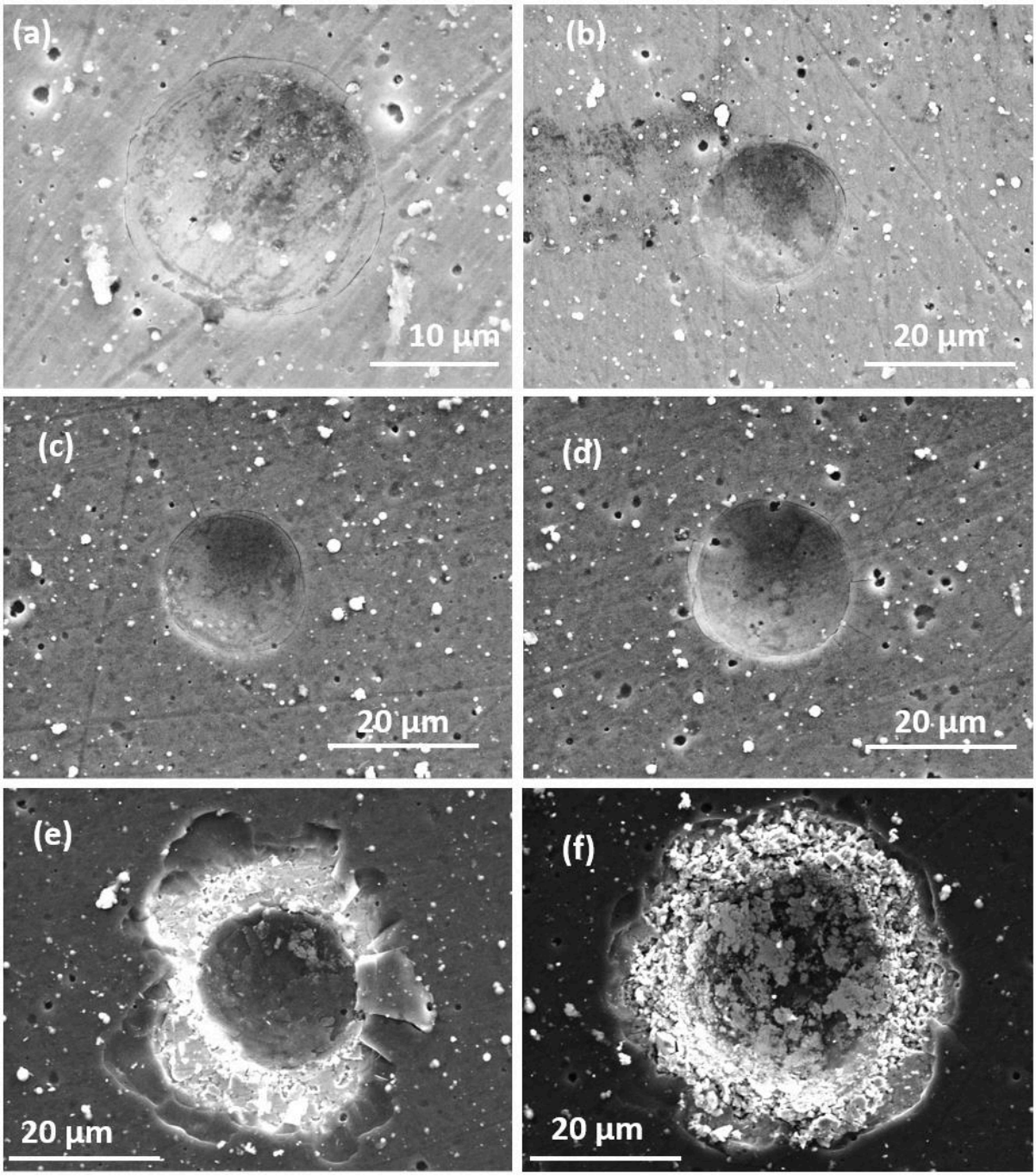

Fig. 1

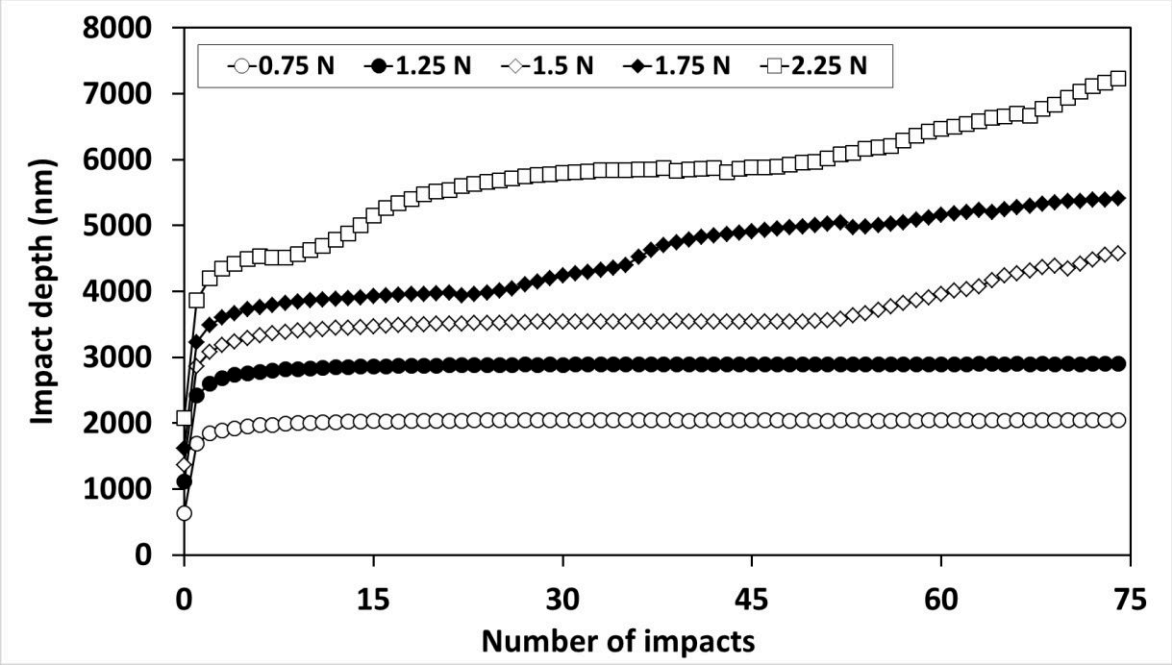
0.75 N
1.25 N
1.5 N
1.75 N
2.25 N
Impact depth (nm)
Number of impacts
0
1000
2000
3000
4000
5000
6000
7000
8000
0
15
30
45
60
75

Fig. 2(a)

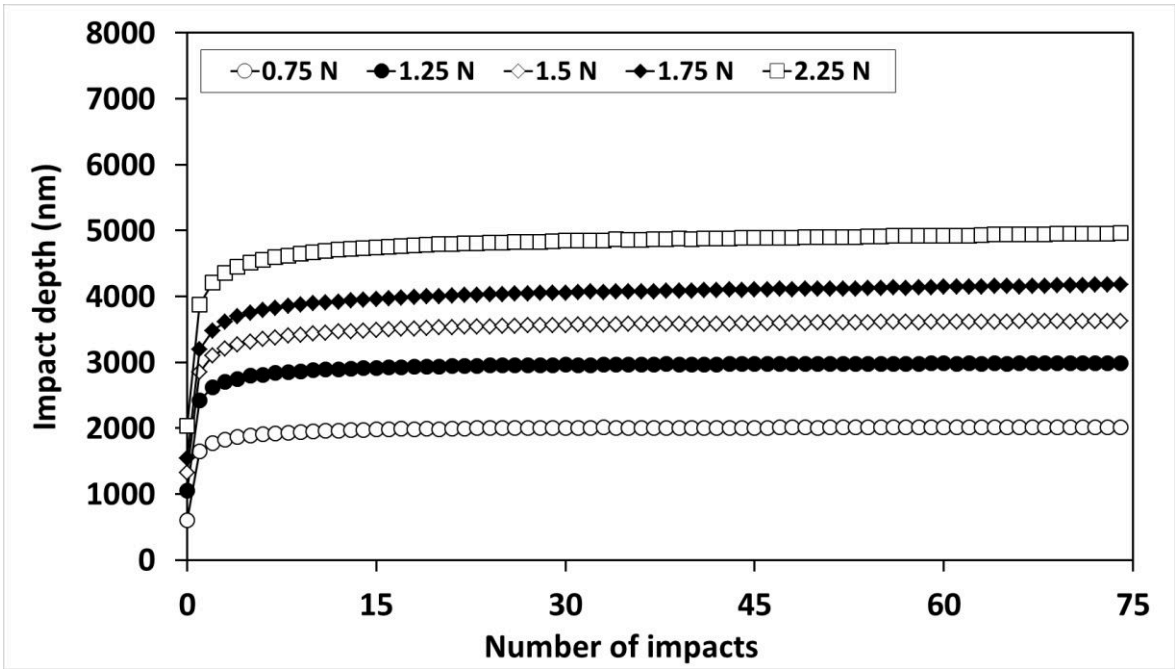
0.75 N
1.25 N
1.5 N
1.75 N
2.25 N
Impact depth (nm)
Number of impacts
0
1000
2000
3000
4000
5000
6000
7000
8000
0
15
30
45
60
75

Fig. 2(b)

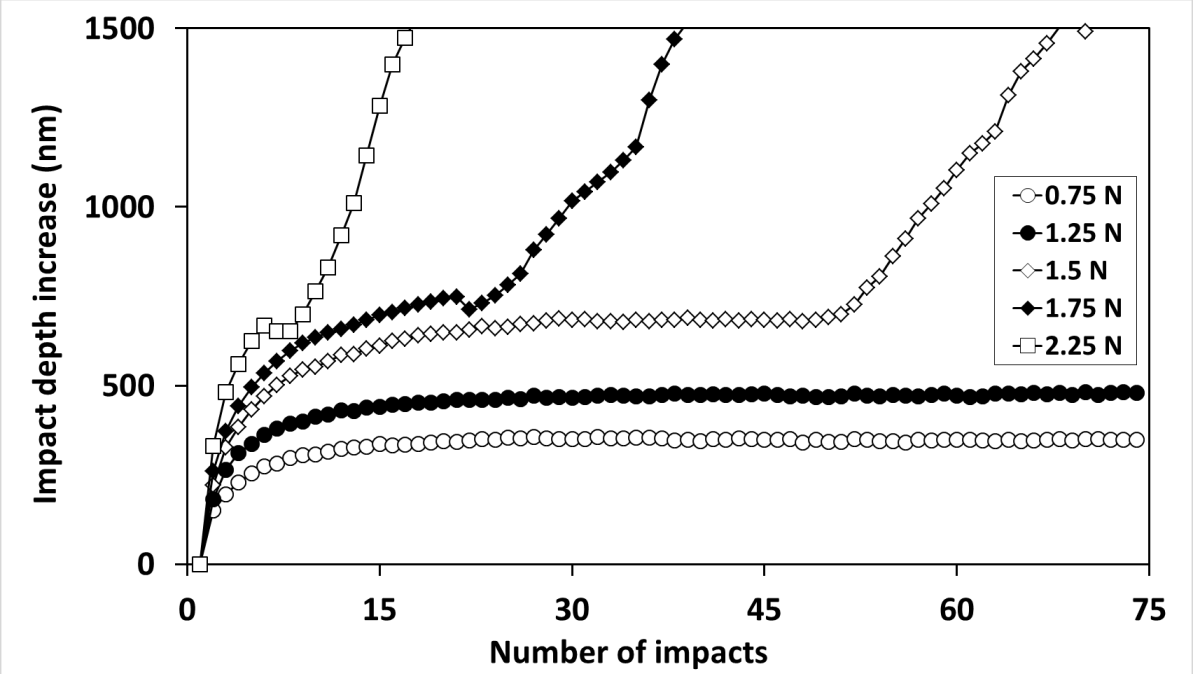
1500
1000
500
0
Impact depth increase (nm)
0
15
30
45
60
75
Number of impacts
0.75 N
1.25 N
1.5 N
1.75 N
2.25 N

Fig. 2(c)

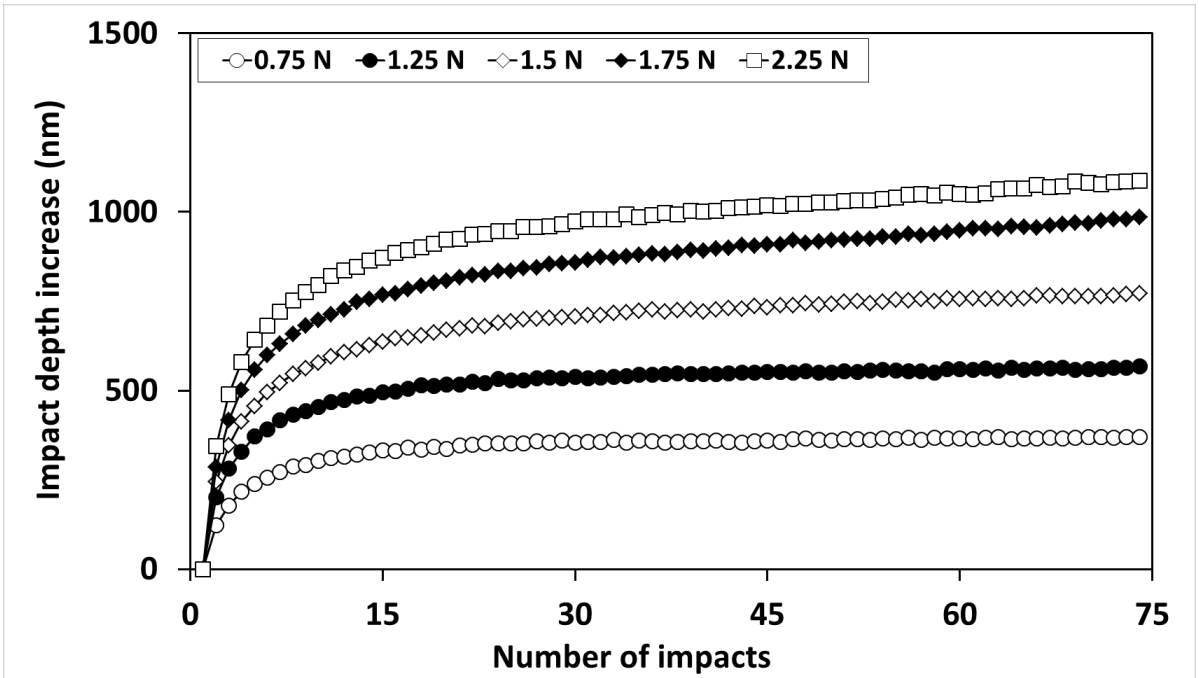
1500
1000
500
0
Impact depth increase (nm)
0
15
30
45
60
75
Number of impacts
0.75 N
1.25 N
1.5 N
1.75 N
2.25 N

Fig. 2(d)

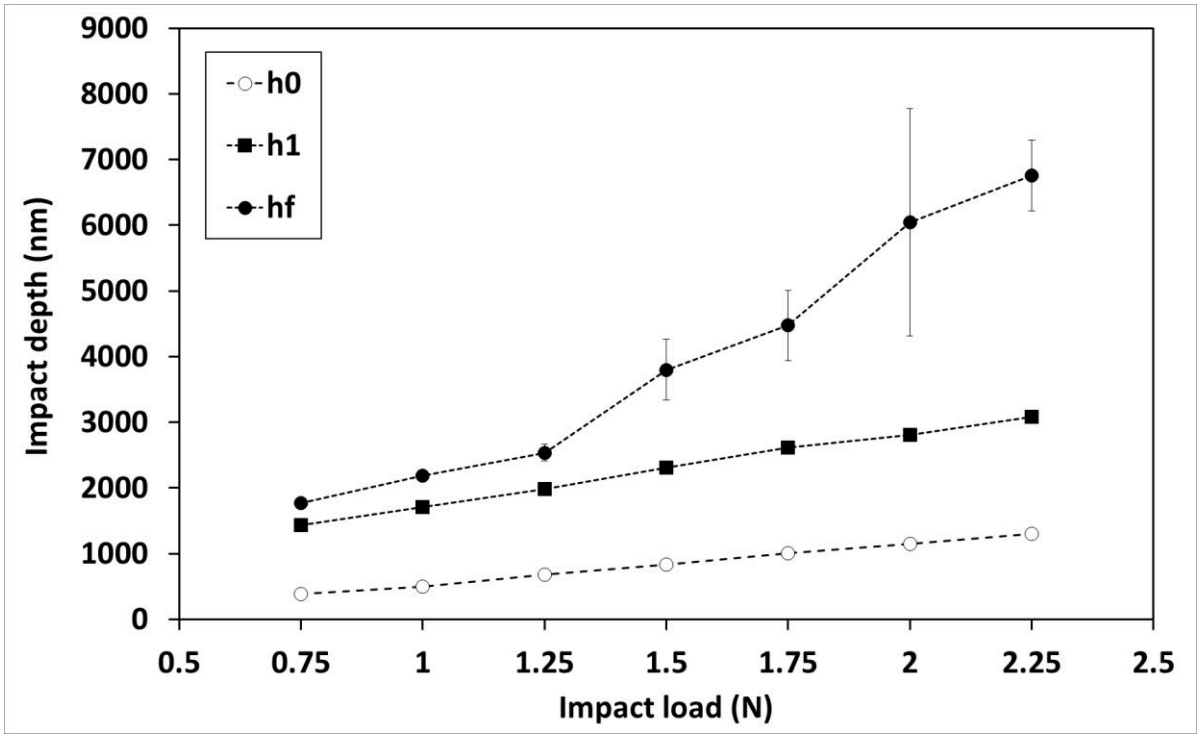
9000
8000
7000
6000
5000
4000
3000
2000
1000
0
Impact depth (nm)
h0
h1
hf
0.5
0.75
1
1.25
1.5
1.75
2
2.25
2.5
Impact load (N)

Fig. 3(a)

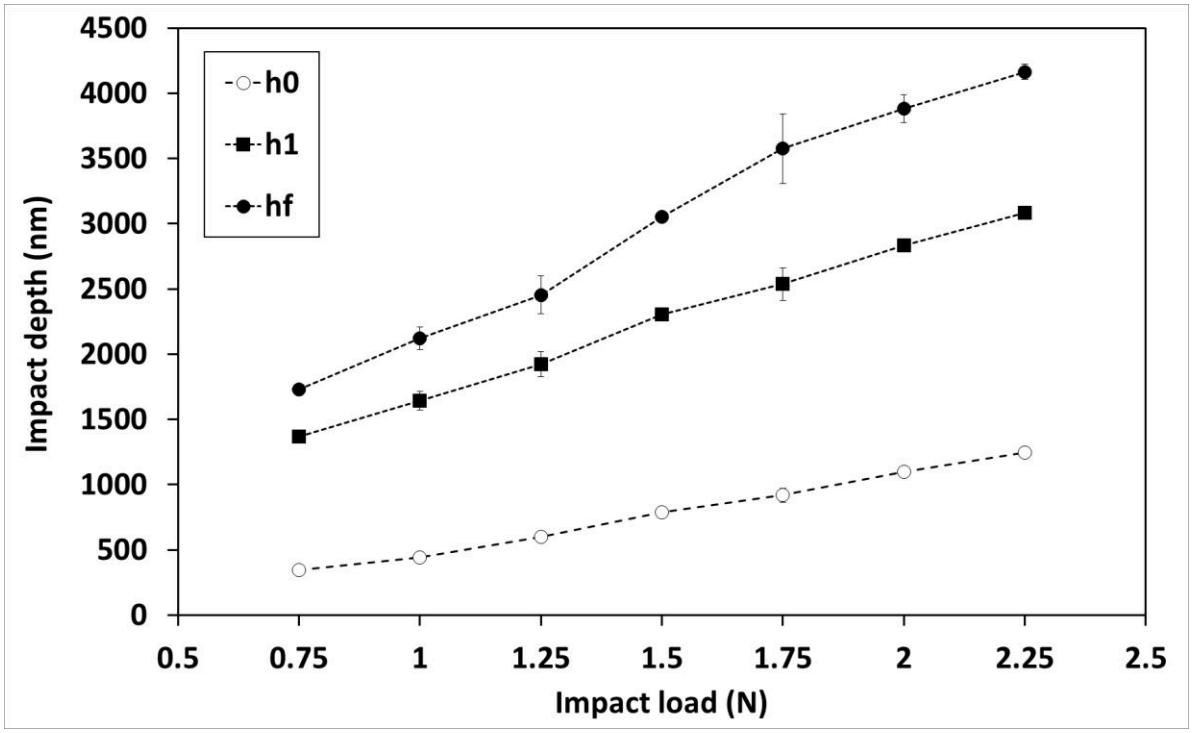
4500
4000
3500
3000
2500
2000
1500
1000
500
0
Impact depth (nm)
h0
h1
hf
0.5
0.75
1
1.25
1.5
1.75
2
2.25
2.5
Impact load (N)

Fig. 3(b)

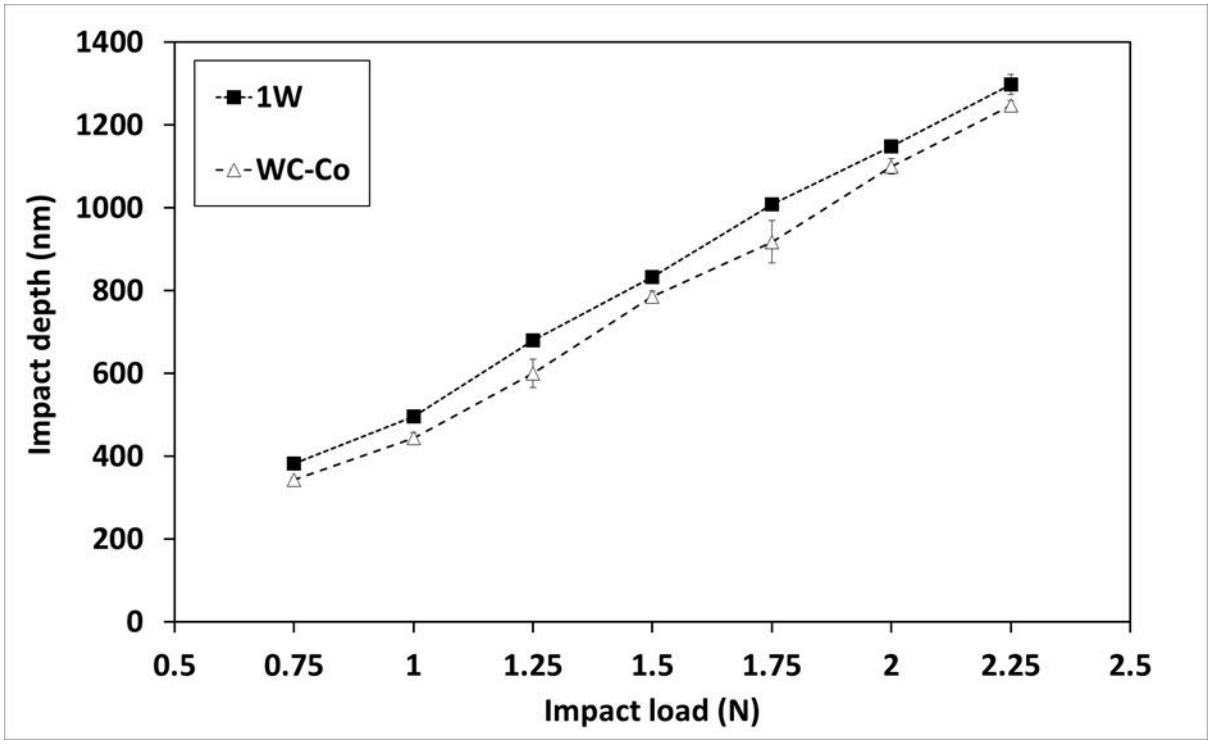
1400
1200
1000
800
600
400
200
0
Impact depth (nm)
1W
WC-Co
0.5
0.75
1
1.25
1.5
1.75
2
2.25
2.5
Impact load (N)

Fig. 3 (c)

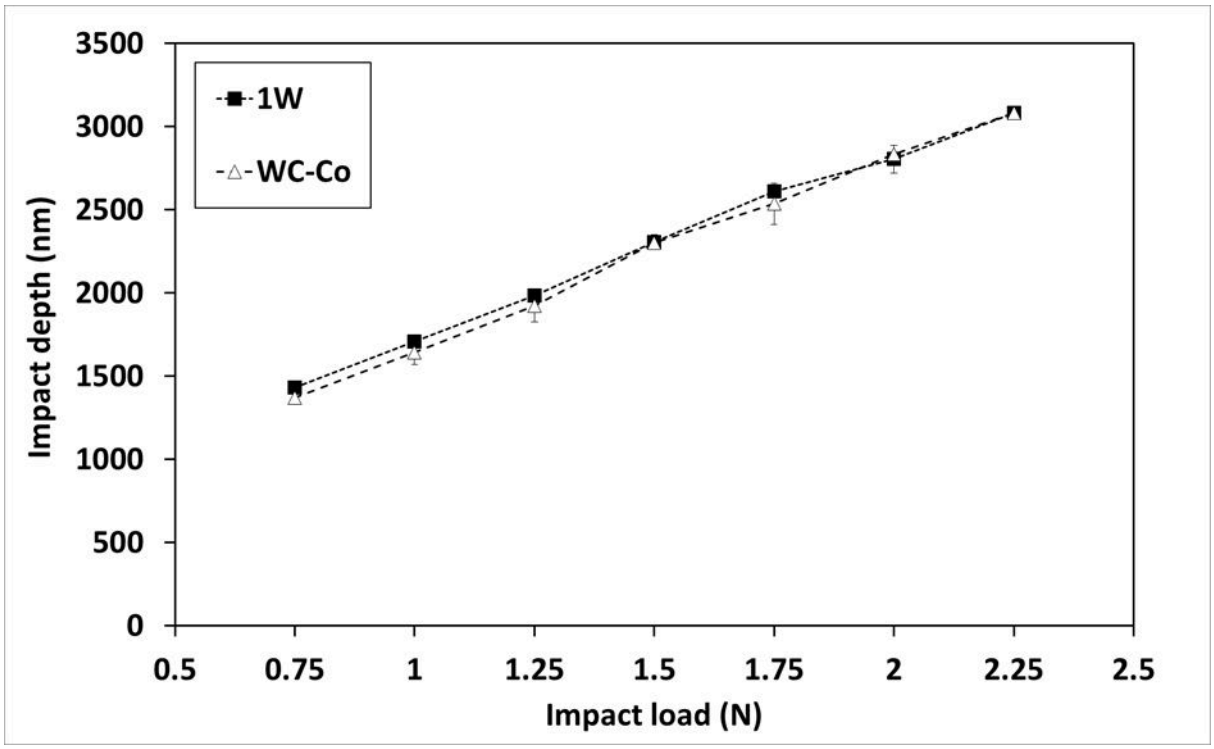
3500
3000
2500
2000
1500
1000
500
0
Impact depth (nm)
1W
WC-Co
0.5
0.75
1
1.25
1.5
1.75
2
2.25
2.5
Impact load (N)

Fig. 3 (d)

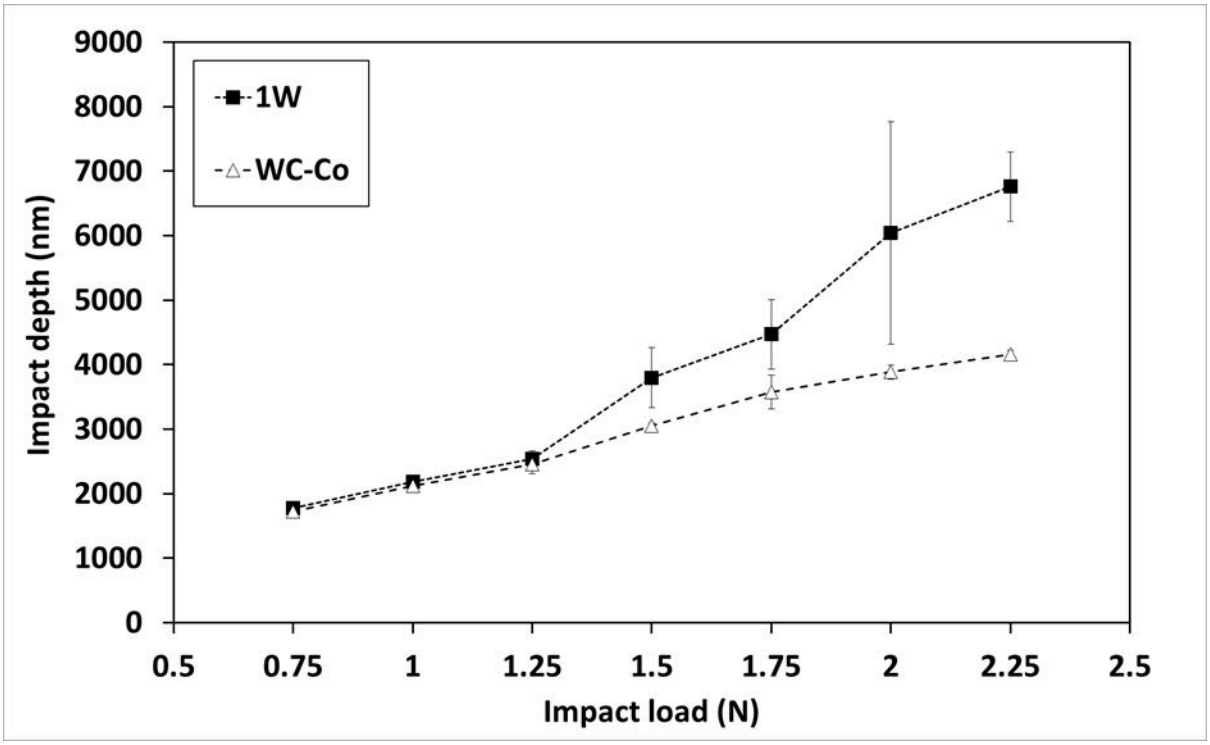

Fig. 3 (e)

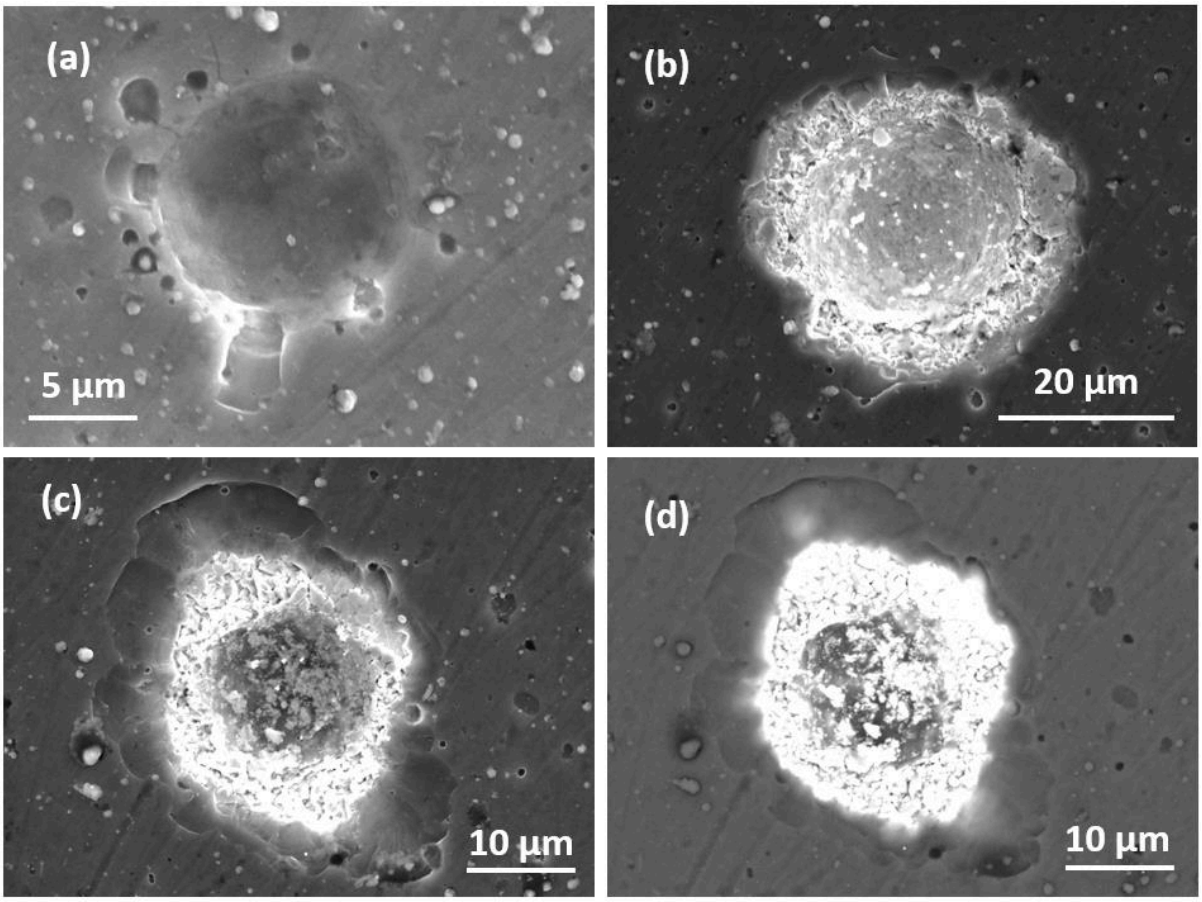

Fig. 4 (a-d)

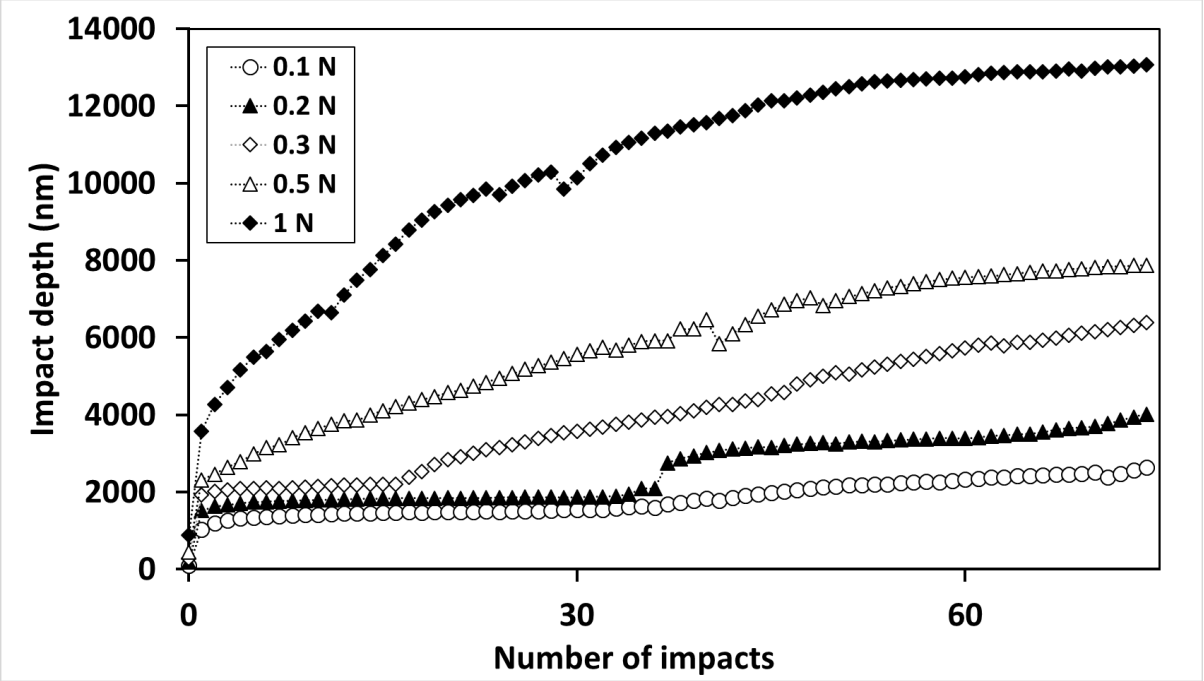
14000
12000
10000
8000
6000
4000
2000
0
Impact depth (nm)
0.1 N
0.2 N
0.3 N
0.5 N
1 N
0
30
60
Number of impacts

Fig. 5.

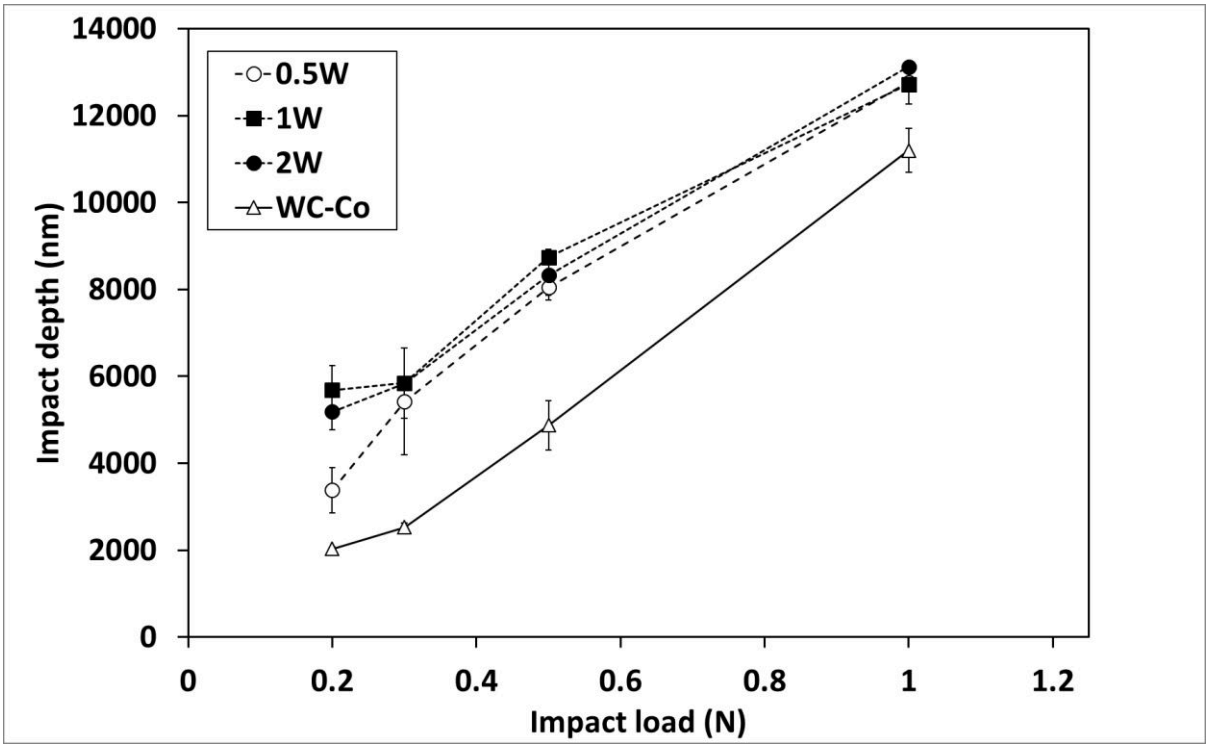
14000
12000
10000
8000
6000
4000
2000
0
Impact depth (nm)
0.5W
1W
2W
WC-Co
0
0.2
0.4
0.6
0.8
1
1.2
Impact load (N)

Fig. 6

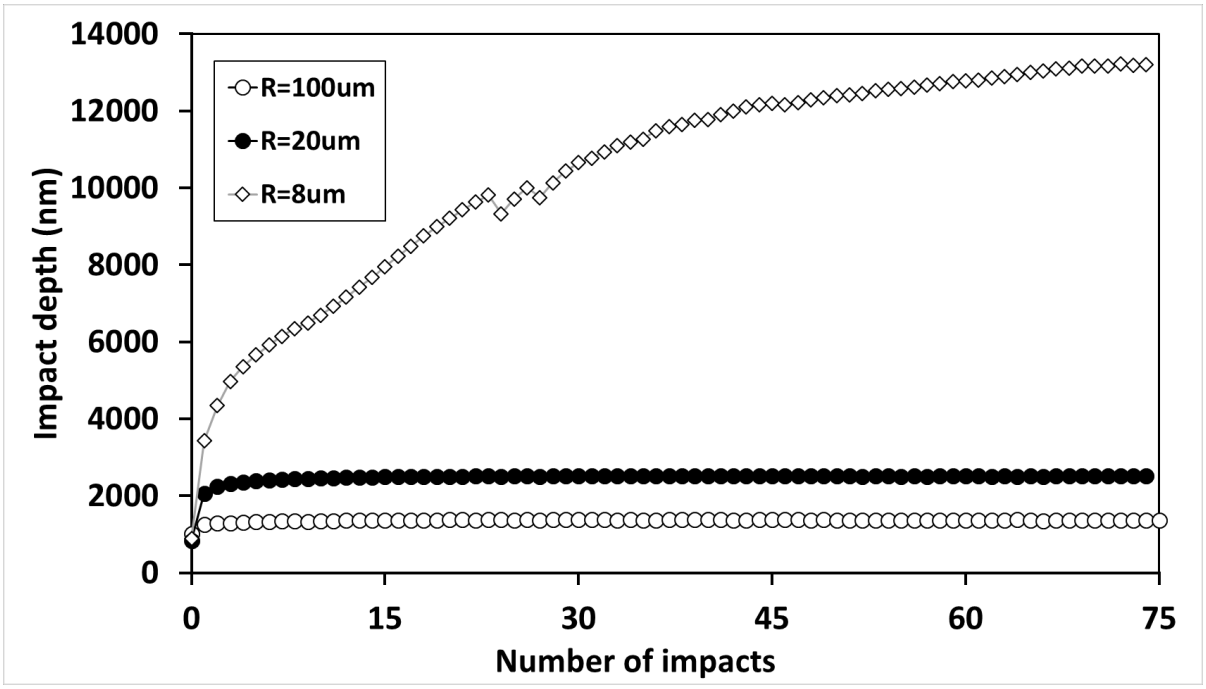
14000
12000
10000
8000
6000
4000
2000
0
Impact depth (nm)
R=100um
R=20um
R=8um
0
15
30
45
60
75
Number of impacts

Fig. 7